Research Article | Vol. 31, No. 7 / 27 Mar 2023 / Optics Express 10978
Optics EXPRESS

Experimental investigation of BDFA-based O-band direct-detection transmission using an optical recirculating loop

YANG HONG,[1,2,*] NATSUPA TAENGNOI,[1] KYLE R. H. BOTTRILL,[1] YU WANG,[1] JAYANTA K. SAHU,[1] PERIKLIS PETROPOULOS,[1] AND DAVID J. RICHARDSON[1]

[1] *Optoelectronics Research Centre (ORC), University of Southampton, Southampton SO17 1BJ, UK*
[2] *Currently with Nokia Bell Labs, Paris-Saclay, Nozay, 91620, France*
[*] *yang.hong@nokia.com*

Abstract: We implemented a bismuth-doped fiber amplifier (BDFA) based optical recirculating loop to investigate the performance of amplified O-band transmission over appreciable distances. Both single-wavelength and wavelength-division multiplexed (WDM) transmission were studied, with a variety of direct-detection modulation formats. We report on (a) transmission over lengths of up to 550 km in a single-channel 50-Gb/s system operating at wavelengths ranging from 1325 nm to 1350 nm, and (b) rate-reach products up to 57.6 Tb/s-km (after accounting for the forward error correction redundancy) in a 3-channel system.

1. Introduction

Driven by data-hungry applications and services such as high-resolution video streaming, virtual reality, and the ever-increasing deployment of the massive Internet of Things, substantial growth in capacity and bandwidth demand have been witnessed in optical networks over recent years, and this trend is predicted to continue in the years to come [1,2]. Consequently, sustained efforts have been made to eke out the achievable capacity of single-mode fibers (SMFs) in the gain region of the erbium-doped fiber amplifier (i.e., the C- and L-bands) to accommodate this growth and help to reduce the risk of a potential capacity crunch. While extensive efforts have been devoted to the development of novel optical fiber types, including multi-core and hollow-core fibers [3–6], which may be impactful in future systems, shorter term solutions that can make use of the already existing infrastructure will also be required. Therefore, further pushing the achievable capacity in installed SMFs is necessary since this will not only extend the lifetime of the existing infrastructure but will also provide a cost-effective way to deal with the increasing data traffic demands [7–13].

To this end, exploring the use of alternative optical windows beyond the C-band is a relevant route, since it offers the potential to realize manyfold capacity enhancement when compared to C-band-only transmission [7–9]. Alongside other candidate wavelengths in which single-mode fiber exhibits a low propagation loss (e.g., the E-, S-, L-, U-bands), the O-band (i.e., 1260 nm - 1360 nm) is an attractive option, since (i) low-cost transceivers operating in this spectral window are already available, and (ii) O-band systems dominate applications in short-reach data transmission which is reflected by the fact that current optical direct detection (DD) access systems are generally implemented in the O-band without optical amplification [14–16]. Therefore, the reach extension of O-band systems has the potential to simplify optical interconnects by reducing the requirement for use of different wavelength bands when transmitting over a wide range of distance scales, and the associated optical-electrical-optical conversions.

#481090 https://doi.org/10.1364/OE.481090
Journal © 2023 Received 16 Nov 2022; accepted 21 Feb 2023; published 17 Mar 2023

Optics EXPRESS

One key obstacle to extending the reach of O-band transmission is that the loss of SMF in this waveband is higher than in the C-band, which necessitates the realization of effective optical amplification technologies [17–19]. At present, semiconductor optical amplifiers (SOAs) represent the mainstream solution for O-band optical amplification. However, these generally suffer from nonlinearity-induced patterning distortions and a relatively poor noise performance [20–23]. To combat the nonlinear patterning effect induced by the SOA, a neural network-based pre-equalizer was used in a 20-km O-band transmission experiment at 50 Gb/s, enabling significant performance improvement in terms of the dynamic range of the receiver [20]. In [21], the adoption of probabilistic shaping was reported in a four-channel O-band wavelength-division multiplexed (WDM) transmission experiment at 280 Gb/s/channel. The corresponding demonstrated reach was 40 km while using both booster and pre-amplifier SOAs [21]. It is clear that despite the use of SOA amplification, these demonstrations did not significantly extend the reach of these systems. Only a few works have been reported in the literature on longer-reach (>40 km) transmission based on SOAs [22,23], and the longest distance ever demonstrated remains 200 km (at 4×10 Gb/s), in which the span length of SMF was 50 km and multiple SOAs were used for in-line amplification [23].

In addition to SOAs, there have been demonstrations of amplified O-band transmission using Raman-, praseodymium-doped- (PDFAs), or bismuth-doped fiber amplifiers (BDFAs) [19,24–32]. In [24,25], distributed/discrete Raman amplifiers were used to extend the reach of passive O-band access systems. However, Raman amplifiers require the transmission of substantial pump power along with the signal in the SMF transmission fiber (in distributed configurations), or suffer from nonlinear signal distortion in the relatively long spool of amplifying fiber required in lumped amplifier configurations, both of which are undesirable [19]. PDFAs which use fluoride-glass doped fibers, on the other hand, can offer relatively high gain and good noise performance over the spectral range specified in O-band telecommunication standards (i.e., around 1310 nm) [19,26,27]. For example, with the help of a PDFA, 2×64-Gb/s O-band transmission was achieved over a 70-km length of SMF [27]. The key drawbacks of PDFAs are however that: (i) they are not based on silica-glass hosts and hence are costly to fabricate and difficult to integrate with silica fiber systems, and (ii) their gain bandwidth is relatively narrow, limiting the number of WDM channels that could potentially be accommodated [19].

More recently, BDFAs have been proposed as a promising route to realizing efficient O-band amplification. Compared to PDFAs, BDFAs adopt a silica glass host and can provide high gain over wide bandwidths (>100 nm), whilst maintaining a good noise figure (NF) [28–32]. Furthermore, unlike SOAs, BDFAs, with their slow gain dynamics, do not introduce nonlinear patterning distortions to the amplified signals, making them suitable for the amplification of high-speed signals [33–36]. Using BDFA-based in-line optical amplification, up to 120-km and 140-km distances were reported in 10-Gb/s/λ O-band CWDM and dense WDM (DWDM) systems, respectively [33]. When using a pair of booster and pre-amplifier BDFAs, a span length of 85 km was achieved in a 25-Gb/s/λ O-band CWDM system [29]. The single-span length was further extended to 100 km for 50-Gb/s/λ transmission using advanced equalization [35]. These prior works clearly indicate the superior performance of BDFAs and highlight their potential for longer-reach O-band transmission.

In this paper, we take a further step in this direction by demonstrating O-band DD transmission over appreciable distances using a BDFA-based optical recirculating loop. In addition to the preliminary results on WDM transmission [36], we further investigate the performance of a single-wavelength configuration considering various modulation formats. Transmission distances up to 550 km (single-wavelength) and rate-reach products up to 57.6 Tb/s-km (WDM) are reported. It is worth mentioning that while in this work we focus on the amplified longer-reach O-band system using DD transmission which is generally considered to be more cost-effective, digital coherent transmission can also be adopted to further increase the capacity and/or reach.

Optics EXPRESS

The associated load for chromatic dispersion (CD) compensation and thus the operation power consumption are expected to be lower than that of a C-band coherent system, since the CD of SMF in the O-band is much lower.

The rest of this paper is organized as follows: In Section 2, investigations of single-wavelength BDFA-based loop transmission between 1325 nm and 1350 nm are presented. Section 3 details scenarios of WDM transmission in the recirculating loop with two different channel spacings. Finally, the conclusion of this work is given in Section 4.

2. Single-wavelength transmission over a BDFA-based optical recirculating loop

We constructed a recirculating loop for operation in the O-band region and carried out DD transmission experiments. To start with, we considered transmission on a single wavelength, which was tuned across the BDFA gain bandwidth.

2.1. Experimental setup

Figure 1 illustrates the experimental setup. A laser that could be tuned between 1325 nm and 1350 nm was used to generate the optical carrier which was modulated in a dual-drive Mach-Zehnder modulator (DD-MZM) driven by an electrical signal generated by an arbitrary waveform generator (AWG). Two separate BDFA units were available in this experiment. The first one (BDFA1) was used at the output of the DD-MZM and served as a booster for the transmitted signal. Subsequently, a variable optical attenuator (VOA1) was used to adjust the optical power to around 11.5 dBm before launching the signal into the optical recirculating loop, which incorporated two O-band acousto-optic modulators (AOMs) (one before the loop and the other within it) and a 50:50 optical coupler. The two AOMs were controlled by two complementary pulses and both exhibited an insertion loss of around 1 dB.

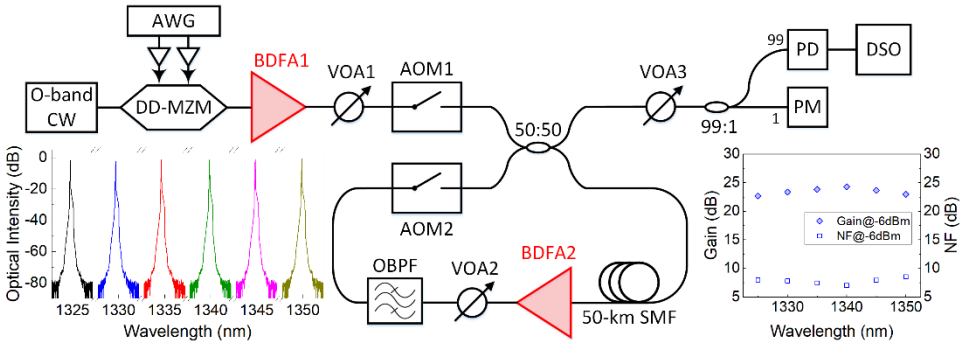

Fig. 1. Experimental setup of the single-wavelength transmission over the BDFA-based optical recirculating loop. Insets: the optical spectra after the DD-MZM in the SSB-QPSK case (left), and the gain and NF performance of BDFA2 at an input power of -6 dBm (right).

In the loop, the optical signal first passed through a span of 50-km SMF and was then amplified by the second BDFA (BDFA2). The loss of the SMF was around 0.32 dB/km at the wavelengths of interest. The zero-dispersion wavelength and the dispersion slope of the adopted SMF were around 1316 nm and 0.083 ps/nm^2/km, respectively. After the in-loop amplification, another VOA (VOA2) was used to account for the gain difference of BDFA2 at different wavelengths and to balance the gain and loss of the loop. Subsequently, an optical bandpass filter (OBPF) with a fixed bandwidth of 1.2 nm was used to suppress the out-of-band noise. The use of this filter was necessary mainly when transmitting data close to the extremities of the BDFA gain bandwidth, where the out-of-band amplified spontaneous emission (ASE) was high. It was removed in the case of the WDM transmission presented later in Section 3. In all wavelength cases the input

Optics EXPRESS

power to BDFA2 was maintained at around -8.6 dBm, which corresponded to the highest optical power that could be achieved across the considered spectral range. For reference, the gain and NF versus wavelength of the in-loop BDFA2 under the input power level of -6 dBm are given in the inset to the bottom-right of Fig. 1. A more detailed characterization of BDFA2, including gain and noise performance, static and dynamic gain tilt, transient response, and polarization dependence, can be found in [37]. We note that limited availability of O-band components prevented us from considering the use of polarization scrambling in this work. Even though not ideal, this is not uncommon among works exploring the early adoption of new technologies [38,39]. Nevertheless, the polarization-dependent loss/gain of the in-loop components was negligible and hence exhibited a minimal impact. It is also worth mentioning that BDFAs can offer high gains over the spectral region specified in O-band telecommunication standards, as has been demonstrated in [19,29,40]. Although the gain profile of the BDFAs used in this work is shifted towards longer O-band wavelengths we consider our experiments to be indicative of the potential of using BDFAs to significantly extend the reach of O-band transmission systems.

After the loop, another VOA (VOA3) was used at the receiver to maintain a fixed received optical power of -3 dBm at the photodetector (PD) in all cases, which was monitored by using a 99:1 optical coupler in front of the PD. Finally, the detected electrical signal was captured by an 80-GSa/s digital storage oscilloscope (DSO) for offline digital signal processing (DSP).

2.2. Offline DSP

We considered three different DD formats for transmission at 50-Gb/s, namely Nyquist 4-ary pulse amplitude modulation (PAM4), capacity-maximized discrete multitone (DMT) using adaptive loading, and Kramers-Kronig detection-assisted single-sideband quadrature phase-shift keying (SSB QPSK).

For 50-Gb/s Nyquist PAM4, after PAM4 mapping, 90-times up-sampling was performed at the transmitter before the application of square-root-raised-cosine filtering (SRRC). The roll-off factor of the SRRC filter was 0.1. Subsequently, the filtered signal was 50-/25-times down-sampled and fed into a 90-GSa/s AWG to generate 25-GBaud Nyquist PAM4 signals. The recorded signal at the DSO went through the synchronization, half-symbol re-sampling, matched SRRC filtering, recursive least-square algorithm-based decision feedback equalization (RLS-DFE) [35,36] and PAM4 de-mapping processes. The recovered binary bits were then compared with the transmitted bits to obtain the corresponding bit error rate (BER) via error counting.

In the case of capacity-maximized DMT, Hermitian symmetry operation-based orthogonal frequency division multiplexing together with the Chow algorithm-based adaptive bit-and-power loading [41] was adopted. The block size of inverse fast Fourier transform (IFFT)/FFT was 512, out of which 200 subcarriers carried data. The analog DMT signal was generated by the AWG operated at 70 GSa/s, which resulted in a signal bandwidth of ~27.34 GHz. Note that QPSK with uniform power loading was used for all data subcarriers in the pilot transmission to estimate their respective signal-to-noise (SNR) conditions, which were then used for adaptive bit-and-power allocation. The target of the adaptive loading was to maximize the achievable transmission capacity while keeping the corresponding BER below the hard-decision forward error correction (HD-FEC) limit of 3.8×10^{-3}.

Since CD has proved to be a limiting factor in longer-reach O-band transmission [29], we also considered 50-Gb/s SSB-QPSK transmission with Kramers-Kronig detection, which facilitates the use of digital CD compensation to eliminate the impact of the CD effect [42]. In the offline implementation of the SSB-QPSK format, after QPSK mapping at the transmitter, the resulting signal was also 90-times up-sampled, after which the in-phase and quadrature components passed through their respective SRRC filters, both of which exhibited a roll-off factor of 0.1. Subsequently, the signals were up-converted to a subcarrier frequency 0.52 times the symbol rate, and then re-combined together before performing 25-times down-sampling and a Hilbert

Optics EXPRESS

transform. Finally, the resulting two signals were fed into a 90-GSa/s AWG to generate the 25-GBaud SSB-QPSK signal. For reference, spectra of the generated optical SSB signals at various wavelengths, captured after the DD-MZM, are given in the bottom-left inset of Fig. 1. At the receiver, the captured signal was first up-sampled before performing Kramers-Kronig detection to recover the in-phase and quadrature components. After that, digital CD compensation was implemented, and synchronization was applied to the resulting signal. This was then re-sampled, filtered with matched SRRC filters, and down-converted, before being equalized by the same RLS-DFE equalizer as used in the Nyquist PAM4 case. Finally, the equalized signal was QPSK de-mapped, after which the BER performance was obtained via error counting.

2.3. 50-Gb/s PAM4 transmission

Figure 2 shows the results of 50-Gb/s Nyquist PAM4 transmission over the O-band recirculating loop. We first investigated the BER performance at 1325-nm, 1340-nm, and 1350-nm wavelengths over different transmission distances (i.e., different numbers of loops). The figure shows that shorter distances were achieved at longer wavelengths, which resulted from the increased severity of the impact of CD [43]. Consequently, the 1325-nm case exhibited the best performance, achieving transmission up to 350-km and 500-km at the HD-FEC (3.8×10^{-3}) and soft-decision FEC (SD-FEC, 2.4×10^{-2}) limits, respectively. These reaches were reduced to ~150 km and 200 km, respectively, when the longer wavelength of 1350 nm was adopted.

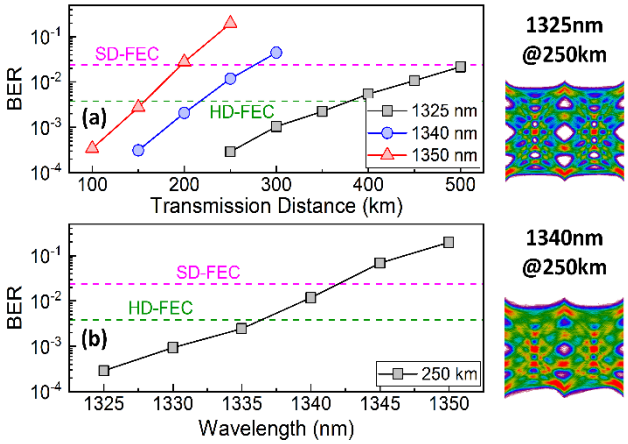

Fig. 2. (a) BER versus transmission distance for 50-Gb/s Nyquist PAM4 transmission over the BDFA-based optical recirculating loop, and (b) BER versus wavelength for the 50-Gb/s Nyquist PAM4 transmission after a 250-km length of SMF. Insets: the recovered PAM4 eye diagrams after 250-km transmission in the 1325-nm and 1340-nm cases.

To further illustrate this point, we measured the BER across the spectral range of interest (i.e., 1325 nm to 1350 nm) after transmission over 250 km (5 loops), and the results are plotted in Fig. 2(b). It is clear that the BER performance degrades with an increase in wavelength. For reference, the corresponding recovered eye diagrams at 1325 nm and 1340 nm are given as insets to Fig. 2.

2.4. Capacity-maximized DMT transmission

The adoption of adaptively-loaded DMT allowed us to evaluate the penalty in transmission capacity as a function of the distance. We therefore, repeated the transmission in the optical recirculating loop using this format. Figure 3 shows the results of achievable capacity versus wavelength for back-to-back (B2B), 200-km (4 loops) and 500-km (10 loops) transmission. Note

Optics EXPRESS

that the achievable capacity here refers to the maximum capacity that can be obtained while keeping the corresponding BER below the HD-FEC limit.

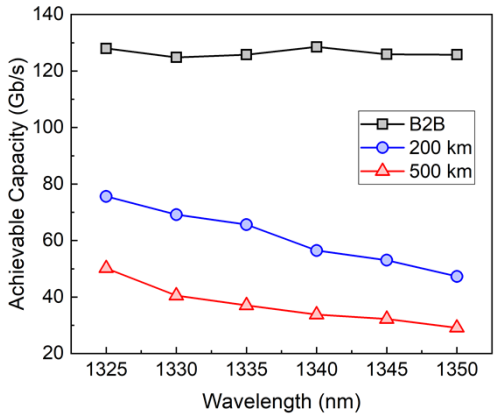

Fig. 3. Achievable capacity versus wavelength for the adaptively-loaded DMT transmission over the O-band BDFA-based optical recirculating loop.

As expected, the achievable capacity (~125Gb/s) was largely independent of wavelength in the B2B case. After 200-km transmission in the SMF, the capacity at the shortest wavelength of 1325 nm was reduced to around 75 Gb/s, due to the joint effects of the noise of the in-loop BDFA2 and CD. In comparison, the capacity at 1350 nm was further reduced to ~50 Gb/s, mainly due to the increased impact of CD at that wavelength. When the transmission reach was extended to 500 km, the achievable capacities at the wavelengths of interest decreased further, ranging between 50 Gb/s and 30 Gb/s, as depicted in the figure.

The impact of CD is directly shown in Fig. 4, which includes the SNR profiles of the 1340-nm transmission in the B2B and 200-km cases. It is seen that compared to the SNR profile in the B2B case, severe power fading was experienced after 200 km, and two spectral nulls appeared around 15 GHz and 25 GHz. These frequencies agree well with the calculated values, when taking into account an average CD value of 2.0 ps/nm/km. (We note that the two low-SNR spikes at ~10 GHz and 20 GHz resulted from clock leakage of the digital-to-analog converter in the AWG used in the experiments [44]). Adaptive bit allocation was performed taking these SNR profiles into account, and the corresponding results are also given in Fig. 4. Clearly, much fewer bits were allocated in the 200-km case, which led to the significantly reduced achievable capacity shown in Fig. 3.

2.5. 50-Gb/s SSB-QPSK transmission

To eliminate the impact of CD in longer-reach O-band transmission, we next adopted the SSB-QPSK format which utilizes Kramers-Kronig detection to recover both the in-phase and quadrature components of the signal, thus facilitating the use of digital CD compensation. Figure 5 shows the results of the 50-Gb/s SSB-QPSK transmission over the BDFA-based O-band optical recirculating loop. It is seen in Fig. 5(a) that the use of SSB-QPSK allows the BER performance differences at the different wavelengths to be substantially reduced, since CD was fully compensated. The minor BER differences are attributed to the colored NF performance of the in-loop BDFA2, which deteriorates slightly towards the edges of the spectral region of interest (see Fig. 1, bottom-right inset).

The BER performance as a function of wavelength for two different distances is shown in Fig. 5(b). Transmission distances of 400 km (8 loops) and 550 km (11 loops) were achieved while keeping the corresponding BERs below the HD- and SD-FEC limits, respectively. To the

Optics EXPRESS

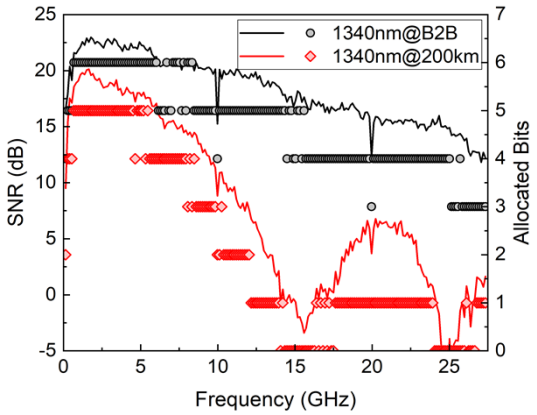

Fig. 4. SNR profiles and the corresponding allocated bits for the 1340-nm transmission in the B2B and 200-km cases.

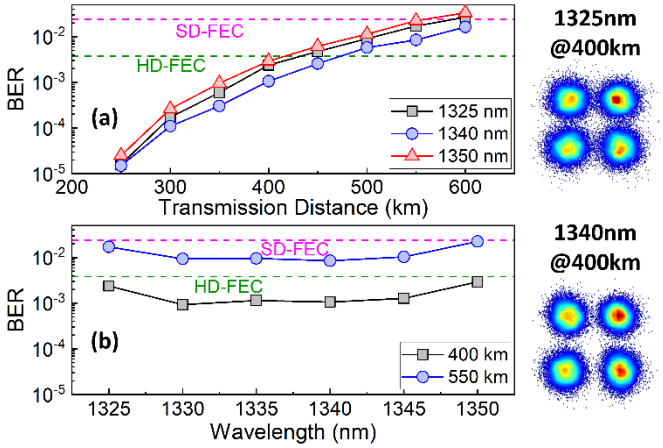

Fig. 5. (a) BER versus transmission distance for 50-Gb/s SSB-QPSK transmission over the BDFA-based optical recirculating loop, and (b) BER versus wavelength for the 50-Gb/s SSB-QPSK transmission after 400-km and 550-km lengths of SMF. Insets: the recovered QPSK constellation diagrams after 400-km transmission in the 1325-nm and 1340-nm cases.

Optics EXPRESS

best of our knowledge, these results represent the longest O-band transmission that has ever been demonstrated to date. For reference, the recovered QPSK constellation diagrams after 400 km at both 1325 nm and 1340 nm are given as insets to Fig. 5.

3. WDM transmission over the BDFA-based optical recirculating loop

In this section, we present WDM experiments with two different channel spacings over the BDFA-based optical recirculating loop to investigate the feasibility of using the BDFA for longer-reach WDM transmission.

3.1. Experimental setup

To facilitate WDM transmission, three lasers were used as the optical carriers, which were fed into two MZMs to modulate odd and even channels independently, thereby ensuring WDM channel decorrelation. Specifically, we considered two WDM cases, with the corresponding wavelengths being (i) 1330.9 nm, 1336.9 nm, and 1343.0 nm, and (ii) 1340.7 nm, 1341.9 nm, and 1343.1 nm, respectively. These correspond to channel spacings of around 6 nm (i.e., 1 THz) in the first case and 1.2 nm (i.e., 200 GHz) in the second, and we will refer to them as CWDM and DWDM respectively in the following. Note that the exact wavelength choice was restricted both by the availability of laser sources for use in this work and the gain bandwidth of the BDFA. After optical modulation, the WDM signals were first combined together via a 50:50 coupler and then amplified by the booster amplifier BDFA1 (this was the same amplifier as in the single-channel experiments), with a total output power of around 13.5 dBm. The powers of the three channels were adjusted to ensure that they were equal at the output of the amplifier. We considered both 50-Gb/s/λ Nyquist OOK and 50-Gb/s/λ SSB-QPSK signals and the corresponding DSP was the same as that detailed in Section 2.2 (the only difference between OOK and PAM4 was that 50-times down-sampling was performed to generate 50-GBaud OOK signals).

We note that only one DD- and one single-drive MZM were available for these experiments. Therefore, we swapped the modulators between odd and even channels, such that only signals generated by the DD-MZM (either Nyquist OOK or SSB-QPSK) were evaluated. This choice was made to ensure a fair comparison between the use of different formats, since only the DD-MZM was able to generate optical SSB signals. Figure 6 shows the optical spectra of the SSB-QPSK WDM signals after the booster BDFA1 for both the CWDM and DWDM transmission cases.

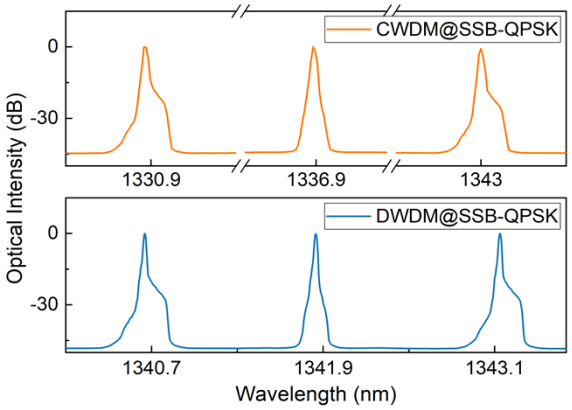

Fig. 6. The optical spectra of the 50-Gb/s/λ SSB-QPSK WDM signals at the transmitter in the CWDM case (upper), and DWDM case (lower).

In the loop, a length of 60 km of SMF was included this time, which exhibited a loss of ~19 dB. The same BDFA2 as in the single-wavelength experiments was used for in-loop amplification, with

Optics EXPRESS

its input power maintained at around -9 dBm (which refers to the total power of the three WDM channels) in both channel spacings that were considered. However, unlike the single-wavelength experiments, the 1.2-nm OBPF was moved to the DD receiver side (i.e. outside the loop) to select the WDM channel under test. The rest of the experimental setup was identical to that detailed in Section 2.1. Note that it was possible to use a longer span length in the WDM loop, both because the BDFAs offered a higher gain in this WDM spectral region and the loop loss was lower after the removal of the OBPF from inside it.

3.2. CWDM transmission

Figure 7 shows the BER versus distance of the 3×50-Gb/s Nyquist OOK CWDM transmission. Similar to the single-wavelength transmission discussed in Section 2, worse BER performance was experienced at the longer-wavelength channels. This performance difference was mainly attributed to the increased severity of CD with increasing wavelength. For reference, the eye diagrams of the recovered signals at the three channels after 240-km (4 loops) transmission are shown in the insets to Fig. 7, through which a gradually degrading quality of the eye diagrams can be observed at longer wavelengths. As a result, to achieve BERs below the SD-FEC limit, the transmission distance needed to be kept below 360 km, 300 km, and 240 km, at the 1330.9-nm, 1336.9-nm, and 1343.0-nm channels, respectively.

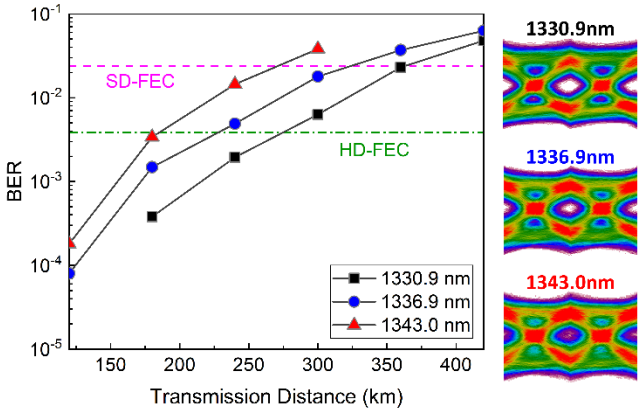

Fig. 7. BER versus transmission distance for the 3×50-Gb/s Nyquist OOK CWDM transmission. Insets: the recovered eye diagrams at the three channels after 240-km SMF transmission.

The degraded performance of the more dispersive channels is further evidenced by a comparison of their detected electrical spectra, as shown in Fig. 8 for the transmission over 240 km. Clearly, the longer-wavelength (i.e., more dispersive) channels suffered a more severe power fading effect, which in turn resulted in the degraded BER performance evidenced in Fig. 7. We have also performed numerical simulations of the CD-induced power fading at the three wavelengths after a 240-km length of SMF, wherein the corresponding dispersion values were assumed to be 1.1, 1.7 and 2.2 ps/nm/km. The results are also presented in Fig. 8 as dashed lines with cross symbols. It is seen that the numerically simulated profiles of the CD-induced power fading agree well with the experimentally captured electrical spectra, confirming that CD represents the key factor that dominates the transmission performance, as discussed above.

To eliminate the impact of CD, we further experimented with the SSB-QPSK format. Figure 9 shows the corresponding BER over the transmission distance for the three CWDM channels. Since the in-loop BDFA2 exhibited colored gain and NF and no gain-equalizing filter was incorporated, the three channels still experienced slightly varying performance. Amongst the

Optics EXPRESS

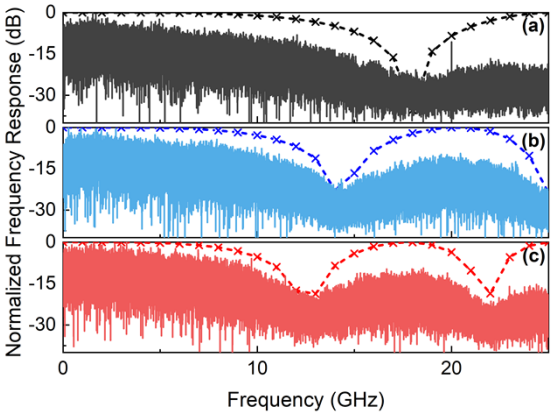

Fig. 8. Electrical spectra of the detected signals after 240-km transmission at the channels of (a) 1330.9 nm, (b) 1336.9 nm, and (c) 1343.0 nm. The dashed lines with cross symbols correspond to the simulation results of the profiles of the CD-induced power fading.

three channels, the central one at 1336.9 nm is seen in Fig. 9 to have achieved the best BER performance; this is where the in-loop BDFA2 exhibited the highest gain and lowest NF (see Fig. 1, bottom-right inset). As a result, reach distances up to 300 km and 600 km were achieved at that wavelength while ensuring that the BER was maintained below the HD- and SD-FEC limits, respectively.

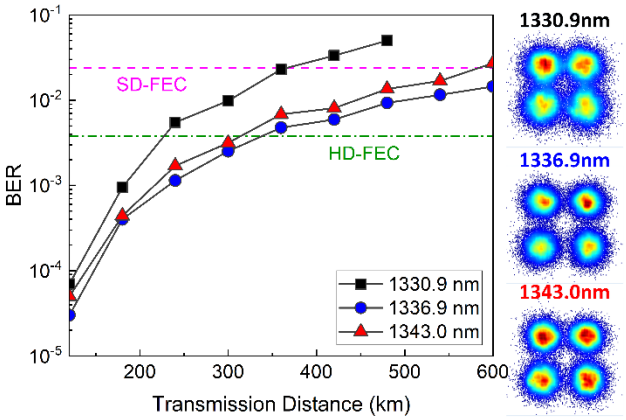

Fig. 9. BER versus transmission distance for the 3 × 50-Gb/s SSB-QPSK CWDM transmission. Insets: the recovered constellation diagrams at the three channels after 360-km SMF transmission.

The worst performance was experienced at 1330.9 nm due to the lower gain of the in-loop BDFA2 at this wavelength. Nonetheless, up to 360-km transmission could still be achieved at the SD-FEC limit. The insets to Fig. 9 present the corresponding recovered QPSK constellation diagrams after a 360-km length of SMF (6 loops).

3.3. DWDM transmission

Finally, we investigated the transmission performance of the BDFA-based optical recirculating loop in a three-channel 50-Gb/s/λ DWDM configuration, wherein both Nyquist OOK and SSB-QPSK were considered. The corresponding results are presented in Fig. 10. Since

Optics EXPRESS

the in-loop BDFA2 offered uniform gain across this narrow spectral window (~2.4 nm) and the corresponding impact of CD was also comparable, all three channels exhibited a similar transmission performance in the Nyquist OOK transmission. As shown in the figure, up to around 180-km and 240-km distances could be achieved at the HD- and SD-FEC limits, respectively. Similarly, comparable BER performance was also experienced at the three channels in the SSB-QPSK case. However, much longer distances were achieved in this case, relative to the Nyquist OOK, thanks to the CD compensation. As shown in Fig. 10, the achievable distances at the HD- and SD-FEC limits were around 300 km and 480 km, respectively. These, to the best of our knowledge, correspond to record rate-reach products in the O-band, amounting to 41.85 Tb/s-km and 57.6 Tb/s-km after accounting for the 7% and 20% redundancy of HD- and SD-FEC, respectively.

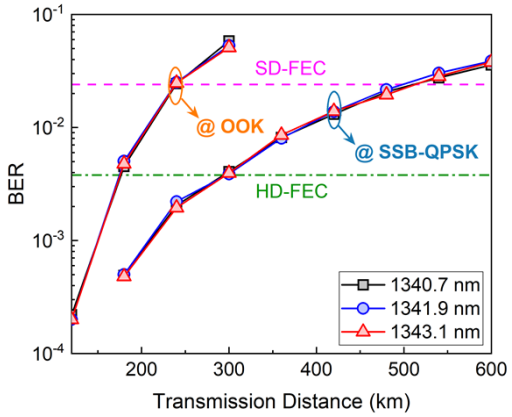

Fig. 10. BER versus transmission distance for the 3 × 50-Gb/s DWDM transmission.

4. Conclusions

In this paper, we have explored the suitability of BDFAs for potential multi-span transmission in the O-band. Through the use of an optical recirculating loop, we have presented transmission experiments in both single-wavelength and WDM configurations with various modulation formats. Specifically, in the single-wavelength case, a 50-Gb/s SSB-QPSK signal was transmitted over 400-km and 550-km distances across the spectral range of 1325 nm to 1350 nm, while having corresponding BERs below the HD- and SD-FEC limits, respectively. For the 3 × 50-Gb/s WDM transmission, both CWDM (~6-nm spacing) and DWDM (~1.2-nm spacing) cases were considered. Distances up to 300 km and 480 km were achieved at the two FEC limits, respectively, which constitute rate-reach products of 41.85 Tb/s-km and 57.6 Tb/s-km after accounting for the respective FEC redundancy. Although clearly still at an early stage, we consider our presented results to highlight that the use of BDFAs may pave the way for longer-reach O-band transmission and could facilitate future implementations of multi-band systems over existing fiber infrastructure.

Funding. Engineering and Physical Sciences Research Council (EP/P003990/1, EP/P030181/1, EP/S002871/1).

Disclosures. The authors declare no conflicts of interest.

Data availability. Data underlying the results presented in this paper are available in Ref. [45].

References

1. E. Agrell, M. Karlsson, A. R. Chraplyvy, D. J. Richardson, P. M. Krummrich, P. Winzer, K. Roberts, J. K. Fischer, S. J. Savory, B. J. Eggleton, M. Secondini, F. R. Kschischang, A. Lord, J. Prat, I. Tomkos, J. E. Bowers, S. Srinivasan, M. Brandt-Pearce, and N. Gisin, "Roadmap of Optical Communications," J. Opt. **18**(6), 063002 (2016).

Optics EXPRESS

2. P. J. Winzer, D. T. Neilson, and A. R. Chraplyvy, "Fiber-optic Transmission and Networking: The Previous 20 and The Next 20 Years," Opt. Express **26**(18), 24190–24239 (2018).
3. S. Beppu, H. Takahashi, T. Gonda, K. Imamura, K. Watanabe, R. Sugizaki, and T. Tsuritani, "56-Gbaud PAM4 Transmission over 2-km 125-μm-Cladding 4-Core Multicore Fibre for Data Centre Communications," in *Proc. of ECOC* (IEEE, 2017), paper Th.2.A.2.
4. D.L. Butler, "Space-Division Multiplexing (SDM) Technology for Short Reach Fiber Optic Systems," in *Proc. of OFC* (Optica, 2016), paper Tu3I.1.
5. D. J. Richardson, N. V. Wheeler, Y. Chen, J. R. Hayes, S. R. Sandoghchi, G. T. Jasion, T. D. Bradley, E. N. Fokoua, Z. Liu, R. Slavik, P. E. Horak, M. N. Petrovich, and F. Poletti, "Hollow Core Fibres and Their Applications," in *Proc. of OFC* (Optica, 2017), paper Tu3H.1.
6. Y. Hong, K. R. H. Bottrill, T. Bradley, H. Sakr, G. T. Jasion, K. Harrington, F. Poletti, P. Petropoulos, and D. J. Richardson, "Low-Latency WDM Intensity-Modulation and Direct-Detection Transmission Over >100 km Distances in a Hollow Core Fiber," Laser Photonics Rev. **15**(9), 2100102 (2021).
7. A. Napoli, N. Calabretta, J.K. Fischer, N. Costa, S. Abrate, J. Pedro, V. Lopez, V. Curri, D. Zibar, E. Pincemin, S. Grot, G. Roelkens, C. Matrakidis, and W. Forysiak, "Perspectives of Multi-band Optical Communication Systems," in *Proc. of OECC* (IEEE, 2018), paper 5B3-1.
8. N. Sambo, A. Ferrari, A. Napoli, N. Costa, J. Pedro, B. Sommerkorn-Krombholz, P. Castoldi, and V. Curri, "Provisioning in Multi-Band Optical Networks," J. Lightwave Technol. **38**(9), 2598–2605 (2020).
9. A. Ferrari, A. Napoli, J. K. Fischer, N. Costa, A. D'Amico, J. Pedro, W. Forysiak, E. Pincemin, A. Lord, A. Stavdas, J. P. F.-P. Gimenez, G. Roelkens, N. Calabretta, S. Abrate, B. Sommerkorn-Krombholz, and V. Curri, "Assessment on the Achievable Throughput of Multi-Band ITU-T G.652.D Fiber Transmission Systems," J. Lightwave Technol. **38**(16), 4279–4291 (2020).
10. X. Liu, A. R. Chraplyvy, P. J. Winzer, R. W. Tkach, and S. Chandrasekhar, "Phase-conjugated Twin Waves For Communication Beyond the Kerr Nonlinearity Limit," Nat. Photonics **7**(7), 560–568 (2013).
11. A. D. Ellis, M. A. Z. Khateeb, and M. E. McCarthy, "Impact of Optical Phase Conjugation on the Nonlinear Shannon Limit," J. Lightwave Technol. **35**(4), 792–798 (2017).
12. T. Fehenberger, A. Alvarado, G. Böcherer, and N. Hanik, "On Probabilistic Shaping of Quadrature Amplitude Modulation for the Nonlinear Fiber Channel," J. Lightwave Technol. **34**(21), 5063–5073 (2016).
13. J. Renner, T. Fehenberger, M. P. Yankov, F. D. Ros, S. Forchhammer, G. Böcherer, and N. Hanik, "Experimental Comparison of Probabilistic Shaping Methods for Unrepeated Fiber Transmission," J. Lightwave Technol. **35**(22), 4871–4879 (2017).
14. F.J. Effenberger, "PON standardisation status and future prospects," in Proc. of ECOC, Dublin, Ireland, paper M.2.F.1, 2019.
15. ITU-G.694.2: Spectral grids for WDM applications: CWDM wavelength grid, ITU Standard (ITU, 2003).
16. Y. Hong, K. R. H. Bottrill, N. Taengnoi, N. K. Thipparapu, Y. Wang, A. A. Umnikov, J. K. Sahu, D. J. Richardson, and P. Petropoulos, "Experimental Demonstration of Dual O + C-band WDM Transmission over 50-km SSMF with Direct Detection," J. Lightwave Technol. **38**(8), 2278–2284 (2020).
17. E. M. Dianov, "Amplification in Extended Transmission Bands using Bismuth-doped Optical Fibers," J. Lightwave Technol. **31**(4), 681–688 (2013).
18. L. Rapp and M. Eiselt, "Optical Amplifiers for Multi–Band Optical Transmission Systems," J. Lightwave Technol. **40**(6), 1579–1589 (2022).
19. V. Mikhailov, J. Luo, D. Inniss, M. Yan, Y. Sun, G.S. Puc, R.S. Windeler, P.S. Westbrook, Y. Dulashko, and D.J. DiGiovanni, "Amplified Transmission Beyond C- and L- bands: Doped Fibre Amplifiers for 1250-1450 nm Range," in *Proc. of ECOC* (IEEE, 2020), paper Mo1E-1.
20. L. Xue, L. Yi, R. Lin, L. Huang, and J. Chen, "SOA Pattern Effect Mitigation by Neural Network based Pre-equalizer for 50 G PON," Opt. Express **29**(16), 24714–24722 (2021).
21. K. Wang, J. Zhang, M. Zhao, W. Zhou, L. Zhao, and J. Yu, "High-speed PS-PAM8 Transmission in a Four-lane IM/DD System using SOA at O-Band for 800 G DCI," IEEE Photon. Technol. Lett. **32**(6), 293–296 (2020).
22. K. Wang, J. Zhang, Y. Wei, L. Zhao, W. Zhou, M. Zhao, J. Xiao, X. Pan, B. Liu, X. Xin, L. Zhang, Y. Zhang, and J. Yu, "100-Gbit/s/λ PAM-4 Signal Transmission over 80-km SSMF based on an 18-GHz EML at O-band," in *Proc. of OFC* (Optica, 2020), paper Th1D.5.
23. J.P. Turkiewicz, M.T. Hill, G.D. Khoe, and H. Waardt, "Cost-effective Transmission Concept for LAN/MAN/SAN Applications," in *Proc. of ECOC* (IEEE, 2005), paper Th1.4.2.
24. B. Zhu, "Entirely Passive Reach Extended GPON using Raman Amplification," Opt. Express **18**(22), 23428–23434 (2010).
25. C. Antony, M. D. Santa, G. Talli, and P. D. Townsend, "Design and Performance Analysis of Raman Amplified XG-PON System," J. Lightwave Technol. **34**(11), 2692–2701 (2016).
26. T. Hayashi, T. Nakanishi, K. Hirashima, O. Shimakawa, F. Sato, K. Koyama, A. Furuya, Y. Murakami, and T. Sasaki, "125-μm-cladding Eight-core Multi-core Fiber Realizing Ultra-high-density Cable Suitable for O-band Short-reach Optical Interconnects," J. Lightwave Technol. **34**(1), 85–92 (2016).
27. F. Gao, S. Zhou, X. Li, S. Fu, L. Deng, M. Tang, D. Liu, and Q. Yang, "2 × 64 Gb/s PAM-4 Transmission over 70 km SSMF using O-band 18G-class Directly Modulated Lasers (DMLs)," Opt. Express **25**(7), 7230–7237 (2017).

Optics EXPRESS

28. N. K. Thipparapu, A. A. Umnikov, P. Barua, and J. K. Sahu, "Bi-doped Fiber Amplifier with a Flat Gain of 25 dB Operating in the Wavelength Band 1320–1360 nm," Opt. Lett. **41**(7), 1518–1521 (2016).
29. V. Mikhailov, M.A. Melkumov, D. Inniss, A.M. Khegai, K.E. Riumkin, S.V. Firstov, F. V. Afanasiev, M.F. Yan, Y. Sun, J. Luo, G.S. Puc, S.D. Shenk, R.S. Windeler, P.S. Westbrook, R.L. Lingle, E.M. Dianov, and D.J. DiGiovanni, "Simple Broadband Bismuth Doped Fiber Amplifier (BDFA) to Extend O-Band Transmission Reach and Capacity," in *Proc. of OFC* (Optica, 2019), paper M1J.4.
30. Y. Wang, N. K. Thipparapu, D. J. Richardson, and J. K. Sahu, "Ultra-Broadband Bismuth-Doped Fiber Amplifier Covering a 115-nm Bandwidth in the O and E Bands," J. Lightwave Technol. **39**(3), 795–800 (2021).
31. S. V. Firstov, A. M. Khegai, A. V. Kharakhordin, S. V. Alyshev, E. G. Firstova, Y. J. Ososkov, M. A. Melkumov, L. D. Iskhakova, E. B. Evlampieva, A. S. Lobanov, M. V. Yashkov, and A. N. Guryanov, "Compact and Efficient O-band Bismuth-Doped Phosphosilicate Fiber Amplifier for Fiber-optic Communications," Sci. Rep. **10**(1), 11347 (2020).
32. Y. Ososkov, A. Khegai, S. Firstov, K. Riumkin, S. Alyshev, A. Kharakhordin, A. Lobanov, A. Guryanov, and M. Melkumov, "Pump-Efficient Flattop O + E-bands Bismuth-Doped Fiber Amplifier with 116 nm –3 dB Gain Bandwidth," Opt. Express **29**(26), 44138–44145 (2021).
33. N. Taengnoi, K. R. H. Bottrill, N. K. Thipparapu, A. A. Umnikov, J. K. Sahu, P. Petropoulos, and D. J. Richardson, "WDM Transmission with In-line Amplification at 1.3 μm using a Bi-Doped Fiber Amplifier," J. Lightwave Technol. **37**(8), 1826–1830 (2019).
34. N. Taengnoi, K. R. H. Bottrill, Y. Hong, N. K. Thipparapu, C. Lacava, J. K. Sahu, D. J. Richardson, and P. Petropoulos, "4-Level Alternate-mark-inversion for Reach Extension in the O-band Spectral Region," J. Lightwave Technol. **39**(9), 2847–2853 (2021).
35. Y. Hong, S. Deligiannidis, N. Taengnoi, K. R. H. Bottrill, N. K. Thipparapu, Y. Wang, J. K. Sahu, D. J. Richardson, C. Mesaritakis, A. Bogris, and P. Petropoulos, "ML-assisted Equalization for 50-Gb/s/λ O-band CWDM Transmission over 100-km SMF," IEEE J. Select. Topics Quantum Electron. **28**(4), 1–10 (2022).
36. Y. Hong, N. Taengnoi, K.R.H. Bottrill, Y. Wang, J.K. Sahu, P. Petropoulos, and D.J. Richardson, "Demonstration of up to 480-km BDFA- Based WDM Direct-Detection Transmission in the O-Band," in *Proc. of ECOC* (IEEE, 2022), paper We4D.3.
37. N. Taengnoi, K. R. H. Bottrill, Y. Hong, Y. Wang, N. K. Thipparapu, J. K. Sahu, P. Petropoulos, and D. J. Richardson, "Experimental Characterization of an O-band Bismuth-doped Fiber Amplifier," Opt. Express **29**(10), 15345–15355 (2021).
38. L. Krzczanowicz, M.A.Z. Al-Khateeb, M.A. Iqbal, I. Phillips, P. Harper, and W. Forysiak, "Performance Estimation of Discrete Raman Amplification within Broadband Optical Networks," in *Proc. of OFC* (Optica, 2019), paper Tu3F.4.
39. S. L. I. Olsson, H. Eliasson, E. Astra, M. Karlsson, and P. A. Andrekson, "Long-haul Optical Transmission Link using Low-noise Phase-sensitive Amplifiers," Nat. Commun. **9**(1), 2513 (2018).
40. Y. Wakayama, D. Elson, V. Mikhailov, R. Maneekut, J. Luo, N. Yoshikane, D. Inniss, and T. Tsuritani, "Over 90-km 400GBASE-LR8 Repeatered Transmission With Bismuth-Doped Fibre Amplifiers," in *Proc. of ECOC* (IEEE, 2022) paper We2A.2.
41. P. S. Chow, J. M. Cioffi, and J. A. C. Bingham, "A Practical Discrete Multitone Transceiver Loading Algorithm for Data Transmission over Spectrally Shaped Channels," IEEE Trans. Commun. **43**(2/3/4), 773–775 (1995).
42. A. Mecozzi, C. Antonelli, and M. Shtaif, "Kramers–Kronig Coherent Receiver," Optica **3**(11), 1220–1227 (2016).
43. Y. Hong, K. R. H. Bottrill, N. Taengnoi, N. K. Thipparapu, Y. Wang, J. K. Sahu, D. J. Richardson, and P. Petropoulos, "Numerical and Experimental Study on the Impact of Chromatic Dispersion on O-band Direct-detection Transmission," Appl. Opt. **60**(15), 4383–4390 (2021).
44. Y. Hong, T. D. Bradley, N. Taengnoi, K. R. H. Bottrill, J. R. Hayes, G. T. Jasion, F. Poletti, P. Petropoulos, and D. J. Richardson, "Hollow-Core NANF for High-Speed Short-Reach Transmission in the S + C+L-Bands," J. Lightwave Technol. **39**(19), 6167–6174 (2021).
45. Y. Hong, N. Taengnoi, K.R.H. Bottrill, Y. Wang, J.K. Sahu, D.J. Richardson, and P. Petropoulos, "Dataset for: Experimental investigation of BDFA-based O-band direct-detection transmission using an optical recirculating loop," University of Southampton Institutional Repository (2023), https://doi.org/10.5258/SOTON/D2543.